DREAM Interrupted: Severing MuvB from DREAM's pocket protein impairs gene repression but not DREAM assembly on chromatin

Paul D. Goetsch[1,2,3,*] and Susan Strome[2]

[1]Department of Biological Sciences, Michigan Technological University, Houghton, MI 49931, USA

[2]Department of Molecular, Cell and Developmental Biology, University of California Santa Cruz, Santa Cruz, CA 95064, USA

[3]Lead contact

*Correspondence:

pdgoetsc@mtu.edu

Summary

The mammalian Retinoblastoma (Rb) protein family, collectively called pocket proteins, regulate entry into and exit from the cell cycle [1-5]. Although pRb plays a dominant role, the Rb-like homologs p130 and p107 represent the ancestral proteins [6, 7] and functionally overlap with pRb to repress cell cycle gene expression during cellular quiescence (G_0) [8-10]. Like pRb, p130 and p107 interact with an E2F-DP transcription factor heterodimer [11-13]. Unlike pRb, they also interact with the highly conserved 5-subunit MuvB complex, forming the DREAM (for Dp, Rb-like, E2F, and MuvB) complex, which mediates transcriptional repression through MuvB [8, 14-17]. To address how the Rb-like pocket protein contributes to MuvB-mediated gene repression, we disrupted the interaction between the sole *Caenorhabditis elegans* pocket protein LIN-35 and the MuvB subunit LIN-52 using CRISPR/Cas9 targeted mutagenesis. Disrupting the LIN-35-MuvB association did not affect DREAM chromatin occupancy but did cause a highly penetrant synthetic multivulval (SynMuv) phenotype, indicating that blocking DREAM assembly impairs MuvB function. Some DREAM target genes became derepressed, indicating that for those genes MuvB chromatin binding alone is not sufficient for gene repression and that direct LIN-35-MuvB association potentiates MuvB's innate repressive activity. Our previous study [17] showed that in worms lacking LIN-35, E2F-DP and MuvB chromatin occupancy is reduced genome-wide. With LIN-35 present, this study demonstrates that the E2F-DP-LIN-35 interaction promotes E2F-DP's chromatin localization, which we hypothesize supports MuvB chromatin occupancy indirectly through DNA. Altogether, this study highlights how the pocket protein family may recruit regulatory factors like MuvB to chromatin through E2F-DP to facilitate their transcriptional activity.

Keywords

DREAM, pocket proteins, MuvB, *Caenorhabditis elegans*, CRISPR/Cas9 genome editing, transcriptional repression

Graphical Abstract

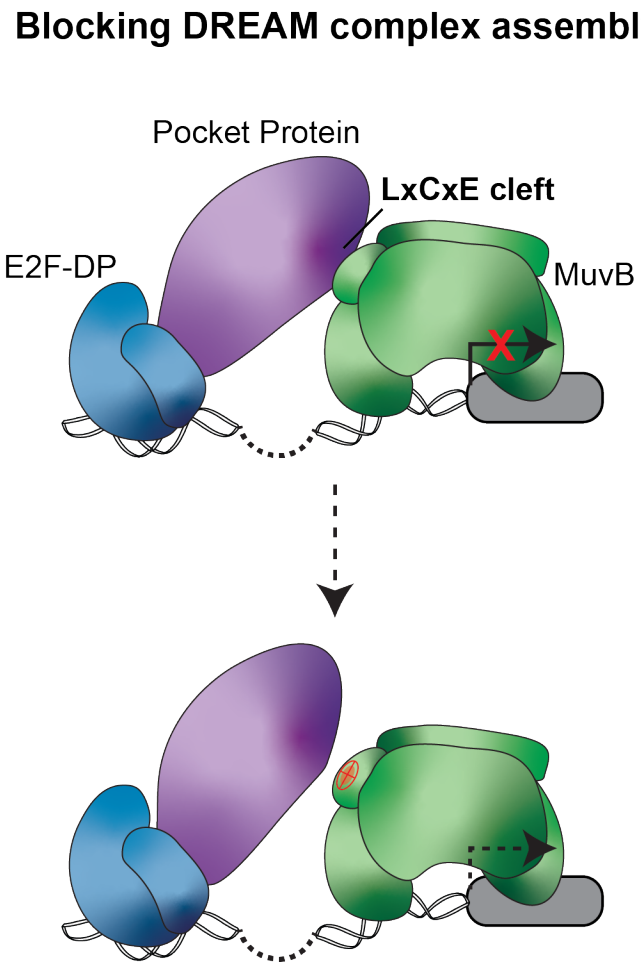

Results and Discussion

The pRb-like pocket proteins (in mammals, p130/p107) interact with repressive E2F-DPs (in mammals, E2F4/5-DP1/2) and a 5-subunit subcomplex called MuvB (in mammals, LIN9, LIN37, LIN52, LIN54, and RBAP48) to form the DREAM transcriptional repressor complex (Figure 1A) [8, 18-20]. E2F-DP and LIN54 direct site-specific chromatin localization [21-25], and the Rb-like pocket protein scaffold serves as a bridge between the 2 DNA-binding DREAM components [18]. The pocket protein-associated complex MuvB, isolated first in *Drosophila melanogaster* [14, 15] and *Caenorhabditis elegans* [16] before homologs were identified in mammals [8, 19, 20], mediates gene repression in the context of DREAM [17]. In *C. elegans*, LIN-35 represents the sole pocket protein, most closely resembling p130/p107 [26]. The *C. elegans* complex, called DRM, similarly regulates cell cycle genes [27], but also regulates cell fate specification by antagonizing Ras signaling during vulval development [16, 28, 29] and by protecting somatic cells from expressing germline genes [30, 31]. We previously reported how LIN-35 loss resulted in a genome-wide decrease in chromatin occupancy of both E2F-DP and MuvB, illustrating how DRM/DREAM disassembly likely proceeds during cell cycle progression [17]. However, our previous findings raised questions about how the pocket protein contributes to DRM/DREAM assembly and function.

Targeted mutagenesis to disrupt DREAM complex formation

Structural studies demonstrated that MuvB interacts with the pocket protein via the LIN52 subunit (Figure 1A) [18]. Using the self-excising cassette (SEC) method for *C. elegans* CRISPR/Cas9 [32], we generated a *lin-52(KO)* strain (*lin52(bn133[lin-52p::TagRFP-T::3xFLAG]*) by completely replacing the *lin-52* gene with *TagRFP-T* coding sequence (Figure 1C). We observed that *lin-52(KO)* rendered worms sterile (Figure 1E), as previously observed in the *lin-52(n3718)* protein null strain [16, 33]. Loss of LIN-9, LIN-53 (*C. elegans* RBAP48), or LIN-54 in protein null strains also renders worms sterile and affects the levels of other MuvB subunits, suggesting that MuvB components require co-expression for assembly/stability of the complex

[16]. Loss of LIN-37 does not cause sterility and does not affect assembly of the rest of MuvB in either *C. elegans* or mammalian cells [16, 34]. We next replaced the *TagRFP-T* coding sequence with *lin-52* tagged with a C-terminal *GFP-3xFLAG* coding sequence, generating the *lin-52(WT)* strain (*lin-52(bn139[lin-52::GFP::3xFLAG]),* Figure 1C). We observed that *lin-52(WT)* completely rescued fertility (Figure 1E), indicating that the GFP tag does not disrupt LIN-52 function.

Since LIN-52 is essential for *C. elegans* fertility, we sought to disrupt the LIN-35-LIN-52 interaction without affecting protein integrity. The mammalian LIN52 protein interacts with the pocket protein LxCxE binding cleft via a suboptimal LxSxExL sequence which is rendered optimal by a nearby S28 phosphorylation site [18] (Figure 1B). S28 phosphorylation by DYRK1A kinase induces formation of mammalian DREAM [35]. In *C. elegans*, the conserved *lin-52* gene encodes the optimal LxCxE sequence (Figure 1B). Additionally, since *C. elegans* lacks a DYRK1A homolog and its corresponding consensus motif RX(X)(S/T)P in LIN-52 (Figure 1B), *C. elegans* DREAM likely does not utilize a phospho-switch to induce DREAM formation [18, 35]. Importantly, the LxCxE binding motif mediates the high-affinity interaction that is employed by the human papillomavirus (HPV) viral oncoprotein E7 to disrupt association of LIN52 with mammalian pocket protein [18]. Therefore, we targeted the LIN-52 LxCxE sequence using CRISPR/Cas9-mediated precision mutagenesis. We generated 2 mutants of the LxCxE binding motif in *lin-52(WT)* using the *dpy-10* co-CRISPR method of small oligo homology-directed repair [36]. We generated the *lin-52(1A)* single alanine mutation strain (*lin-52(bn150[lin-52[C44A]::GFP::3xFLAG)*) and the *lin-52(3A)* triple alanine mutation strain (*lin-52(bn151[lin-52[L42A,C44A,E46A]::GFP::3xFLAG)*) with the intent to completely disrupt LIN-52's interaction with the *C. elegans* pocket protein LIN-35 (Figure 1D). Additional silent mutations were included in the oligo repair templates to generate new restriction enzyme cut sites to aid in genotyping (Figure 1D).

Full loss of *C. elegans* DREAM activity causes sterility, as observed in protein null mutants of worm E2F-DP (*dpl-1* and *efl-1)* and worm MuvB (*lin-9, lin-52, lin-53, and lin-54)* [37-39]. Since the C-terminally GFP-tagged *lin-52* coding sequence completely rescued *lin-52(KO)* sterility, we

were able to test whether *lin-52(1A)* and *lin-52(3A)* disrupt DREAM function. We observed that neither the 1A nor 3A mutation in the LIN-52 LxCxE sequence caused a significant reduction in brood size (Figure 1E). Using western blot analysis of selected DREAM components from *lin-52(WT)* and mutant lysates, we observed that DREAM component protein levels were unaffected compared to N2 (Bristol) (Figure 1F, Figure S1). Similarly, using live image analysis of *lin-52(WT), lin-52(1A),* and *lin-52(3A)* L4 larvae, we observed that LIN-52 level and localization appeared normal in mutants (Figure 1C). Together, these results demonstrate that mutation of the LIN-52 LxCxE sequence does not cause a *lin-52* null phenotype and does not alter the levels and tissue distribution of MuvB components.

Blocking DREAM complex formation recapitulates the classic SynMuv phenotype

C. elegans DREAM components were initially identified in genetic screens for a Synthetic Multivulval (SynMuv) phenotype [16, 26, 33, 40]. All 8 components of DREAM were classified as SynMuv B genes; double mutant worms bearing a mutation in a SynMuv B gene along with a mutation in a SynMuv A gene have multiple vulvae along their ventral body instead of the usual single vulva [41]. We hypothesized that if DREAM function was affected by mutation of LIN-52's LxCxE sequence, then pairing our 1A and 3A LIN-52 mutations with a SynMuv A mutation should generate a SynMuv phenotype. SynMuv A alleles *lin-8(n2731)* [42] or *lin-15A(n767)* [43] resulted in a SynMuv phenotype when paired with *lin-52(3A)* but not with *lin-52(1A)* or as expected with *lin-52(WT)* (Figure 2A). These results indicate that the triple alanine substitution of LxCxE affects DREAM function.

To test whether the triple alanine substitution in fact impaired pocket protein-MuvB association, we performed co-immunoprecipitations (co-IPs) from protein extracts prepared from *lin-52(WT)*, *lin-52(1A)*, and *lin-52(3A)* late embryos. We pulled down LIN-35 and tested for LIN-52 association using the GFP epitope, and we pulled down LIN-52 using either the GFP or FLAG epitope and tested for LIN-35 association (Figure 2B, Figure S2). In both co-IP experiments, we observed that LIN-52 association with LIN-35 was lost in *lin-52(3A)* extracts but not in *lin-52(1A)*

extracts. These results demonstrate that the LIN-52 triple alanine substitution successfully severed the protein-protein association between LIN-52 and LIN-35, effectively blocking formation of an intact DREAM complex.

E2F-DP-LIN-35 and MuvB subcomplexes independently co-occupy chromatin sites

In the absence of LIN-35, E2F-DP and MuvB do not associate with one another and their chromatin occupancy is reduced genome-wide [17]. In our *lin-52(3A)* worm strain, LIN-35 is present, but its association with MuvB is severed. We tested the impact of this severing on the chromatin localization of DREAM components using chromatin immunoprecipitation (ChIP). We chose 4 genes, *set-21, mis-12, polh-1,* and *air-1,* as representative DREAM target genes; in *lin-35* null embryos, the chromatin occupancy of DREAM components was greatly diminished at each of their gene promoters [17]. Importantly, DREAM component chromatin occupancy was undetectable at the *air-1* promoter in the absence of LIN-35 [17]. We observed that all tested DREAM components remained similarly enriched at the 4 selected promoters in *lin-52(3A)* as compared to *lin-52(WT)* (Figure 3A). An additional 6 DREAM target gene promoters were tested and showed similar DREAM occupancy profiles (Figure S3A). This included *C. elegans* E2F-DP (DPL-1 and EFL-1) and LIN-35, suggesting that the chromatin association of the repressive E2F-DP transcription factor heterodimer is stabilized by its interaction with the pocket protein.

To test whether MuvB and E2F-DP-LIN-35 co-occupy DREAM target regions, we performed sequential ChIP analysis. We first ChIPed LIN-52 via its FLAG tag and then ChIPed LIN-35. We observed no significant difference in LIN-35 co-occupancy in *lin-52(3A)* extracts vs. *lin-52(WT)* extracts (Figure 3B). Our results indicate that, although the interaction of LIN-35 and MuvB is disrupted, DREAM components nevertheless co-localize at target promoters through their respective protein-DNA interactions. We previously observed that in the absence of LIN-35, E2F-DP and MuvB protein-DNA interactions were not sufficient for robust chromatin localization [17]. Importantly, *in vitro* analysis of heterodimeric mammalian E2F-DP complexes identified a distinct induction of DNA bending, especially in the case of the homologues of *C. elegans* EFL-1-

DPL-1 (E2F-4/DP-1/2) [44]. Therefore, we propose that DREAM-associated E2F-DP heterodimers promote MuvB co-occupancy through a DNA bending-dependent mechanism. Together, our results suggest a model in which the LIN-35 pocket protein promotes E2F-DP chromatin occupancy, which in turn promotes MuvB chromatin occupancy.

Severing the LIN-35-MuvB connection impairs transcriptional repression of some but not all DREAM target genes

MuvB dissociation from E2F-DP-LIN-35 resulted in no observed loss in chromatin occupancy of DREAM at the 10 gene promoters tested (Figure 3A, Figure S3A). Each of the gene products targeted by the 4 selected promoter regions in Figure 3A was upregulated in the *lin-35* null strain [17, 45]. We performed gene expression analysis of these 4 genes in *lin-52(WT)*, *lin-52(1A)*, and *lin-52(3A)* late embryos using RT-qPCR (Figure 3C). We observed that 2 genes, *set-21* and *polh-1*, were significantly upregulated in both *lin-52* mutant strains, while 2 genes, *mis-12* and *air-1*, were not up-regulated. Transcript levels of each of the gene products targeted by the 6 selected promoter regions in Figure S3A were not affected (Figure S3B). Importantly, *air-1* upregulation in the *lin-35* null strain was accompanied by complete loss of MuvB promoter association [17]. Thus, MuvB chromatin occupancy is necessary but not sufficient for repression of DREAM target genes. Our findings reveal that the LIN-35-MuvB association potentiates MuvB-mediated transcriptional repression but is not required.

Outlook and Future Work

The trio of pocket proteins, pRb, p107, and p130, govern cell cycle exit and reentry through targeted transcriptional repression of cell cycle genes. We analyzed how the *C. elegans* Rb-like pocket protein LIN-35 contributes to the formation and function of the DREAM complex, which relies on the recruitment of the highly conserved and essential 5-subunit MuvB complex to direct target gene repression. Using CRISPR/Cas9-mediated targeted mutagenesis, we generated a mutant *C. elegans* strain in which MuvB's LIN-35-interacting subunit LIN-52 was rendered incapable of interacting with LIN-35. This LIN-52 mutant recapitulated the classic Synthetic

Multivulval phenotype observed in all *C. elegans* DREAM mutants that perturb its ability to repress genes. We determined that while LIN-35 and MuvB association was lost, the LIN-35 and E2F-DP occupancy on chromatin was unchanged. Additionally, even without direct protein-protein association, MuvB co-occupied sites with the heterotrimeric E2F-DP-LIN-35 complex. Our results highlight that the pocket protein stabilizes E2F-DP chromatin occupancy, which we hypothesize in turn supports MuvB occupancy potentially through local alteration of DNA shape.

Our results support an exciting model for how local E2F-DP-mediated alterations to DNA shape enhanced by their interaction with a pocket protein promote MuvB co-occupancy. Even with evolutionary divergence from the ancestral pocket protein, this model may also apply to pRb function. Many histone deacetylases and chromatin remodeling complexes associate with pRb through the LxCxE binding cleft, although many of these associations have only limited support thus far from structural/biochemical interaction studies [46]. Variation in pRb monophosphorylation events that can alter pRb structure and recognition of binding partners offered one explanation for how pRb can potentially interact with >300 individual protein partners [47, 48]. Our data provide an alternative, but not exclusive, mechanism for how direct and stable pRb association with these complexes may be unnecessary. Perhaps pRb association with E2F-DPs promotes localization of these complexes to genomic sites. Additional dissection of DREAM and pRb structure and function will shed light on how the pocket proteins mediate their essential cellular roles.

Acknowledgments

We thank Seth Rubin and members of the Rubin and Strome labs for helpful discussions. Some strains were provided by the Caenorhabditis Genetics Center, which is funded by the NIH Office of Research Infrastructure Programs (P40 OD010440). This work was supported by National Institutes of Health R01 grant GM34069 to S.S. and American Cancer Society Postdoctoral Fellowship PF-16-106-01-DDC to P.D.G.

Author Contributions

Conceptualization, P.D.G and S.S. Methodology, P.D.G. Investigation, P.D.G. Writing – Original Draft, P.D.G. Writing – Review & Editing, P.D.G. and S.S. Funding Acquisition, P.D.G. and S.S. Resources, P.D.G. Supervision, S.S.

Declaration of Interests

The authors declare no competing interests.

Figure Legends

Figure 1 Targeted mutagenesis to disrupt DREAM complex formation

(A) Model of *C. elegans* DREAM complex bound to DNA: E2F-DP (blue), the pocket protein LIN-35 (purple), and the 5-subunit MuvB subcomplex (green). The highlighted region shows the target region for this study: an LxCxE binding motif in the MuvB subunit LIN-52 that interacts directly with the LIN-35 pocket protein.

(B) Alignment of *H. sapiens* LIN52 and *C. elegans* LIN-52 sequences. The human LxSxExL and worm LxCxE sequences are highlighted in yellow, and the human DYRK1A consensus phosphorylation sequence is highlighted in orange. Arrows indicate residues involved in the interaction with the pocket protein.

(C) Live worm fluorescence images of *lin-52(KO), lin-52(WT*), *lin-52(1A),* and *lin-52(3A)* L4 larvae. Composites were artificially straightened. Scale bar, 100μM.

(D) Sanger sequencing of *lin-52* LxCxE coding region in *lin-52(WT), lin-52(1A*), and *lin-52(3A*).

(E) Strip chart of the brood sizes of Bristol (N2), *lin-52(KO)*, *lin-52(WT)*, *lin-52(1A)*, and *lin-52(3A)*. Significance (** p-value < 0.01) was determined by a Wilcoxon-Mann-Whitney test comparing indicated strains to Bristol (N2).

(F) Western blot analysis of DREAM subunits LIN-52 (via GFP tag), EFL-1, LIN-35, and LIN-37 using whole worm lysates from Bristol (N2)*, lin-52(WT), lin-52(1A),* and *lin-52(3A)* separated by SDS/PAGE. Antibodies used are indicated on the right. Alpha-tubulin was used as a loading control. Full blots are shown in Figure S1

Figure 2 Blocking DREAM complex formation recapitulates the classic SynMuv phenotype

(A) Table indicating the percentage Synthetic Multivulval (SynMuv) penetrance of *lin-52(WT), lin-52(1A)*, and *lin-52(3A)* in combination with SynMuv A mutant alleles *lin-8(n2731)* or *lin-15A(n767)* with standard deviation indicated. Population size (n*)* indicated in parentheses.

(B) Late embryo extracts from *lin-52(WT)*, *lin-52(1A)*, and *lin-52(3A)* were immunoprecipitated with anti-LIN-35, anti-GFP, and anti-FLAG antibodies, with no antibody serving as a negative control. Proteins bound (B) and unbound (UB) were separated by SDS/PAGE, and western blot analysis was performed using the antibodies indicated on the right. 5% of Input (In) was included. Asterisks indicate non-specific bands. Full blots are shown in Figure S2.

Figure 3 Analysis of chromatin association with and repression of DREAM target genes

(A) ChIP-qPCR of 5 DREAM subunits DPL-1, EFL-1, LIN-37, LIN-35, and LIN-52 (via GFP tag) from *lin-52(WT*) (white) and *lin-52(3A*) (black) late embryo extracts at 4 DREAM target genes. IgG was used as a negative control. Signals are presented as percentage of Input DNA. Error bars indicate standard error of the mean. Additional target genes are shown in Figure S3.

(B) Sequential ChIP-qPCR of LIN-52 (via FLAG tag) followed by LIN-35 or IgG from *lin-52(WT*) (white) and *lin-52(3A*) (black) late embryo extracts at 4 DREAM target genes. Signals are presented as percentage of FLAG IP DNA. Error bars indicate standard error of the mean.

(C) RT-qPCR analysis comparing transcript levels of the 4 DREAM target genes in *lin-52(WT)* (white) *lin-52(1A)* (grey), and *lin-52(3A)* (black) late embryos. Expression values from 2 independent experiments each consisting of 4 biological replicates were averaged and are presented as the relative quantity (Rq) compared to *act-2.* Error bars indicate standard error of the mean, and significance was determined by a student's T-test between transcript levels in mutant (3A or 1A) vs WT (** p-value < 0.01). Additional target genes are shown in Figure S3.

Figure S1

Full western blots of DREAM subunits LIN-52 (via GFP tag), EFL-1, LIN-35, and LIN-37 using whole worm lysates from Bristol (N2)*, lin-52(WT), lin-52(1A),* and *lin-52(3A)* separated by SDS/PAGE. Antibodies used are indicated below each blot. Alpha-tubulin was used as a loading

control. Membranes were cut at the 75 kDa band. Arrows indicate blot regions presented in Figure 1F.

Figure S2

Full western blots of late embryo extracts from *lin-52(WT)*, *lin-52(1A)*, and *lin-52(3A)* that were immunoprecipitated with anti-LIN-35, anti-GFP, and anti-FLAG antibodies, with no antibody serving as a negative control. Proteins bound (B) and unbound (UB) were separated by SDS/PAGE and transferred to PVDF membranes that were cut at the 75 kDa band (indicated by dashed line). Antibodies used are indicated below each blot. 5% of Input (In) was included. Arrows indicate blot regions presented in Figure 2B.

Figure S3

(A) ChIP-qPCR of 5 DREAM subunits DPL-1, EFL-1, LIN-37, LIN-35, and LIN-52 (via GFP tag) from *lin-52(WT*) (white) and *lin-52(3A*) (black) late embryo extracts at 6 DREAM target genes. IgG was used as a negative control. Signals are presented as percentage of Input DNA. Error bars indicate standard error of the mean.

(B) RT-qPCR analysis comparing transcript levels of the 6 DREAM target genes in *lin-52(WT)* (white) *lin-52(1A)* (grey), and *lin-52(3A)* (black) late embryos. Expression values from 2 independent experiments each consisting of 4 biological replicates were averaged and are presented as the relative quantity (Rq) compared to *act-2.* Error bars indicate standard error of the mean.

Methods

Contact for Reagent and Resource Sharing

Requests for information, strains, and reagents should be directed to and will be fulfilled by Paul D. Goetsch (pdgoetsc@mtu.edu)

Experimental Model and Subject Details

Strains were cultured on Nematode Growth Medium (NGM) agarose plates with *E. coli* OP50 and incubated at 20°C. Experiments were performed on embryos, L4 larvae, and young adult

hermaphrodites as indicated, with males used for genetic crosses. Genotyping of genome edited strains and progeny of subsequent genetic crosses was performed on single worm lysates using standard techniques with primers indicated in the Key Resources Table (Table 1).

Method Details

CRISPR/Cas9-mediated genome editing

To generate *lin-52(KO),* 2 Cas9 target sites were identified near the 5' and 3' ends of the gene using the MIT CRISPR design tool (http://crispr.mit.edu). The 20 nucleotide crDNA targeting sequences were cloned into the PU6::unc119_sgRNA vector (Addgene plasmid #46169) using the overlapping PCR fragment method described in [49]. The *lin-52* KO homologous repair template was generated by amplifying homology arms containing the *lin-52* promoter and *lin-52* 3' UTR and cloned into the N-terminal tag digested pDD284 vector (Addgene plasmid #66825) using Glibson Assembly (New England Biolabs) [50], as described in [32]. The following CRISPR/Cas9 and co-injection marker [51] plasmid mix was microinjected into the germline of ~50 N2 young adults: 50 ng / µL Cas9 expression plasmid (pDD162, Addgene #47549), 2.5 ng / µL Pmyo-2::mCherry::unc-54utr (pCJF90, Addgene #19327), 5 ng / µL Pmyo-3::mCherry::unc-54utr (pCFJ104, Addgene #19328), 10 ng / µL pRAB-3::mCherry::unc-54utr (pGH8, Addgene #19359), 50 ng / µL lin-52 5' sgRNA (pPDG14), 50 ng / µL lin-52 3' sgRNA (pPDG18), and 10 ng / µL lin-52p::TagRFP-T^SEC^3xflag::lin-52 3' UTR (pPDG13). CRISPR/Cas9-positive progeny were treated with hygromycin and screened for the Roller phenotype and absence of fluorescent co-injection marker expression (the latter eliminates false-positive extrachromosomal arrays). Individuals from 1 positive selection plate were selected and balanced to create the strain SS1240 *lin-52(bn132(lin-52p::TagRFP-T^SEC^3xflag::lin-52 3' UTR)) III / hT2G [bli-4(e937) let-?(q782) qIs48] (I;III)* [52]. The self-excising cassette (SEC) was removed by a 4-5 hour heat-shock of L1 larvae at 32°C. Non-Roller F1 progeny were isolated to create the strain SS1241 *lin-52(bn133(lin-52p::TagRFP-T::3xflag::lin-52 3' UTR)) III / / hT2G [bli-4(e937) let-?(q782) qIs48] (I;III).*

To generate *lin-52(WT)*, 2 Cas9 target sites were identified near the 5' and 3' ends of the *TagRFP-T-3xFLAG* coding sequence using the MIT CRISPR design tool. The 20 nucleotide crDNA targeting sequences were cloned into the pDD162 vector using the Q5 Site Directed Mutagenesis Kit (New England Biolabs), as described in [53]. The *lin-52* WT homologous repair template was generated by amplifying homology arms containing the *lin-52* promoter with the gene's coding sequence and the *lin-52* 3' UTR and cloned into the C-terminal tag digested pDD282 vector using Gibson Assembly, as described in [32]. The following CRISPR/Cas9 and co-injection marker plasmid mix was microinjected into the germline of ~50 SS1241 young adults: 50 ng / µL TagRFP-T 5' sgRNA-Cas9 vector (pPDG21), 50 ng / µL TagRFP-T 3' sgRNA-Cas9 vector (pPDG22), 2.5 ng / µL pCJF90, 5 ng / µL pCFJ104, and 10 ng / µL lin-52p::lin-52 CDS-GFP^SEC^3xflag::lin-52 3' UTR (pPDG17). CRISPR/Cas9-positive progeny were treated with hygromycin and screened for the Roller phenotype and absence of fluorescent co-injection marker expression. Individuals from 2 of 3 positive selection plates were selected and made homozygous to create strains SS1325 and SS1326 *lin-52(bn138(lin-52::GFP^SEC^3xflag)) III*. The SEC was removed by heat-shock, and non-Roller F1 progeny were isolated to create the strains SS1256 and SS1257 *lin-52(bn139(lin-52::GFP::3xflag)) III*. SS1256 was backcrossed 6 times to generate strain SS1272, which was used in downstream experiments.

To generate *lin-52(1A)* and *lin-52(3A)*, 1 Cas9 target site was identified near the LxCxE coding sequence using the MIT CRISPR design tool and cloned into the pDD162 vector, as described above. Single strand DNA templates included at least 40 base pairs of homology flanking the LxCxE coding sequence and silent mutations to aid genotyping, as illustrated in Figure 1C. The following/Cas9 and co-injection marker plasmid mix was microinjected into the germline of 6 (for 1A) and 10 (for 3A) SS1256 young adults: 40 ng / µL lin-52 LxCxE sgRNA-Cas9 vector (pPDG59), 2.5 ng / µL pCJF90, 5 ng / µL pCFJ104, 20 ng / µL lin-52 mutagenesis ssDNA template (1A or 3A), 40 ng / µL *dpy-10(cn64)* sgRNA (pJA58, Addgene plasmid #59933), and *dpy-10(cn64)* ssDNA template. *dpy-10(cn64)* guide and ssDNA template were co-injected to

select for positive CRISPR activity in injectant progeny, as described in [36]. Injected adults were cloned onto individual plates, and F1 progeny were screened for presence of a Roller (Rol) and/or Dumpy (Dpy) phenotype. Individual Rol and/or Dpy progeny were genotyped, resulting in 3 independent *lin-52(1A*) and 2 independent *lin-52(3A)* strains. Each strain was backcrossed 6 times to create SS1273-SS1275 *lin-52(bn150(lin-52[C44A]::GFP::3xflag)) III,* and SS1276 and SS1277 *lin-52(bn151(lin-52[L42A,C44A,E46A]::GFP::3xflag)) III*. SS1273 and SS1276 were used in downstream experiments.

Microscopy

L4 larvae were mounted on a 10% agarose pad and immobilized with a 1-2 µL suspension of 0.1 µm polystyrene beads (Polysciences), as described in [54]. Fluorescence images were acquired using a Solamere spinning-disk confocal system with µManager software [55]. The microscope setup was as follows: Yokogawa CSUX-1 spinning disk scanner, Nikon TE2000-E inverted stand, Hamamatsu ImageEM X2 camera, solid state 405-, 488-, and 561-nm laser lines, 435–485, 500–550, and 573–613 fluorescent filters, and Nikon Plan Fluor 40x air objective. Images were processed using Image J [56].

***C. elegans* phenotype scoring**

For brood size analyses, L4 individuals were cloned to fresh plates every 24 hours and all progeny were counted. For SynMuv phenotype scoring, 3 replicate plates per strain were set up with 5-10 adults that were allowed to lay eggs for 6 hours. Progeny were incubated at 20°C for 3 days, then scored for the presence or absence of pseudovulvae. The percentages of multivulva worms in each replicate population were averaged, and the standard deviation was calculated.

Immunoblotting and co-immunoprecipitation (coIP)

For immunoblotting whole worm lysates, 200 adults from each strain were picked into SDS gel-loading buffer (50 mM pH 6.8 Tris-Cl, 2% sodium dodecyl sulfate, 0.1% bromophenol blue, 100 mM β-mercaptoethanol). For coIP, embryos collected after bleaching gravid worms were aged for 3.5 hours before freezing them in liquid nitrogen. Lysates were prepared by grinding

frozen embryos using a mortar and pestle, resuspending in lysis buffer (25 mM HEPES pH 7.6, 150 mM NaCl, 1mM DTT, 1mM EDTA, 0.5 mM EGTA, 0.1% Nonidet P-40, 10% glycerol) with Complete EDTA-free Protease Inhibitors (Roche), and sonicating twice for 30 seconds. Lysates were clarified and precleared using a mix of Protein A and Protein G Dynabeads (ThermoFisher). Protein concentrations of coIP lysates were determined using a Qubit fluorometer (ThermoFisher). For each IP, 5 µg of anti-FLAG was crosslinked to Protein G Dynabeads and 2 µg of anti-GFP or anti-LIN-35 was crosslinked to Protein A Dynabeads using dimethyl pimelimidate in 0.2 M trimethylamine pH 8.2. Crosslinking was stopped using 0.1M Tris pH 8.0, and beads were washed with 0.1 M glycine pH 2.8 before being stored in phosphate buffered saline pH 7.2 with 0.05% Tween-20. For each IP, 8 mg of protein lysate was mixed with antibody-conjugated Dynabeads and incubated for 2 hours at 4°C. Each IP was washed with lysis buffer, and eluted with 50 µL 2x SDS gel-loading buffer for 5 minutes at 98°C

Proteins were separated by SDS/PAGE, and western blot analysis was performed using a 1:1,000-1:5000 dilution of primary antibody and 1:2,000 dilution of an appropriate HRP-conjugated secondary antibody. Serial western blot analysis was performed by stripping the blot with buffer containing 0.2M pH 2.2 glycine, 0.1% SDS, and 1% Tween-20 between antibody probings.

Chromatin immunoprecipitation (ChIP) and sequential ChIP

Embryos collected after bleaching gravid worms were aged for 3.5 hours before freezing them in liquid nitrogen. Lysates were prepared by grinding, crosslinking for 10 minutes in 1% formaldehyde, and sonicating to an average size of 250 base pairs in FA buffer (50 mM HEPES/KOH pH 7.5, 1 mM EDTA, 1% Triton X-100, 0.1% sodium deoxycholate, 150 mM NaCl) using a Bioruptor (Diagenode) on the high setting with 60 rounds of 30 seconds on and 1 minute rest. Protein concentrations of lysates were determined using a Qubit fluorometer.

For ChIP, chromatin extracts were precleared with Protein A Dynabeads. ChIPs were performed with 2 mg of extract and 1 µg of antibody, with 2% of the extract set aside for an input

reference control. ChIPs were incubated overnight at 4°C with 1% sarkosyl. Protein A Dynabeads equilibrated in 20 µL FA buffer were added and incubated for 2 hours at 4°C. ChIPs were washed with the following buffers: once with FA buffer containing 1 M NaCl, once with FA buffer containing 0.5 M NaCl, once with TEL buffer (10 mM Tris-HCl pH 8.0, 0.25 M LiCl, 1% NP-40, 1% sodium deoxycholate, 1 mM EDTA), and twice with TE buffer (10 mM Tris-HCl pH 8.0 and 1 mM EDTA). 2 elutions of 50 µL elution buffer containing TE plus 1% SDS and 250 mM NaCl were incubated at 55°C. Eluted ChIP and input samples were incubated with proteinase K for 1 hour at 55°C. Crosslinks were reversed overnight at 65°C. DNA was purified by phenol-chloroform extraction and ethanol precipitation using glycogen as a carrier. Quantitative PCR was performed using SYBR green reagents on an Applied Biosystems ViiA 7 Real-Time PCR System (ThermoFisher).

For sequential ChIP, chromatin extracts were precleared with Protein G Dynabeads and 4 parallel ChIPs per replicate were performed with 2.5 mg of extract and 2.5 µg of anti-FLAG antibody, with 2% of the extract set aside for an input reference control. ChIPs were incubated overnight at 4°C with 1% sarkosyl. Protein G Dynabeads equilibrated in 20 µL FA buffer were added and incubated for 2 hours at 4°C. ChIPs for each replicate were washed as described above and pooled. 2 elutions of 50 µL 0.1M $NaHCO_3$ plus 1% SDS were incubated at 55°C for 15 minutes. Elutions were divided, diluted with FA buffer with 1% sarkosyl, and incubated with anti-LIN-35 or IgG as a negative control, with 10% of the elution set aside as a reference control. The 2^{nd} ChIP was incubated overnight at 4°C. Protein A Dynabeads equilibrated in 20 µL FA buffer were added and incubated for 2 hours at 4°C. ChIPs were washed and eluted twice with 50 µL elution buffer with incubation at 55°C. Eluted ChIP, reference, and input samples were incubated with proteinase K for 1 hour at 55°C. Crosslinks were reversed overnight at 65°C. DNA was purified by phenol-chloroform extraction and ethanol precipitation using glycogen as a carrier. Quantitative PCR was performed similarly to above.

Analysis of transcript levels by RT-qPCR

Embryos collected after bleaching gravid worms were aged for 3.5 hours before freezing them in Trizol for RNA isolation. A total of 1 µg RNA was treated with DNase and reverse transcribed using the High Capacity cDNA Kit (Applied Biosystems). qPCR was performed using SYBR green reagents on an Applied Biosystems ViiA 7 Real-Time PCR System (ThermoFisher). The relative quantity of experimental transcripts was calculated with *act-2* as the control gene using the ΔCt method.

Quantification and statistical analysis

For brood size analysis, significance was determined using a Wilcoxon-Mann-Whitney test comparing CRISPR/Cas9-genome edited strains to N2 (Bristol). For ChIP-qPCR and transcript level analysis by RT-qPCR, significance was determined using a student's T Test between *lin-52(WT)* and *lin-52(1A)* and *lin-52(3A).*

Figure 1

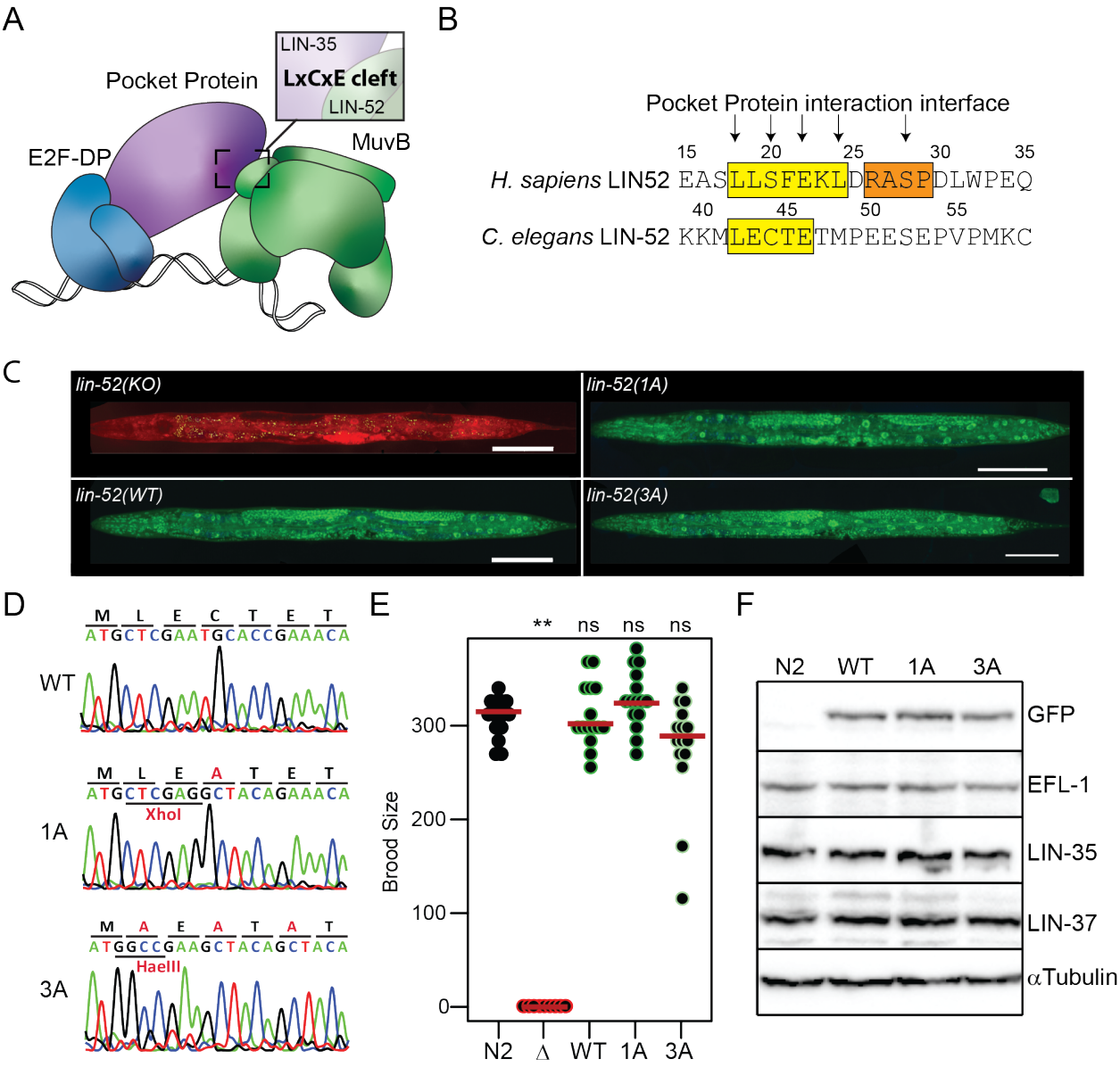

Figure 2

A

% SynMuv±s.d. (n)	*lin-8(n2731)*	*lin-15A(n767)*
WT	0±0 (382)	0±0 (505)
1A	0±0 (211)	0±0 (422)
3A	99.3±0.6 (301)	96.5±0.2 (375)

B

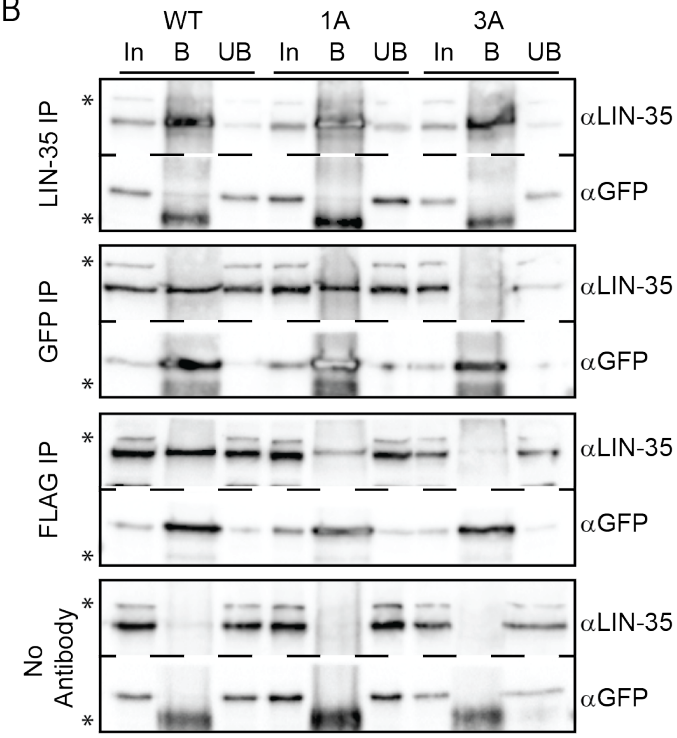

Figure 3

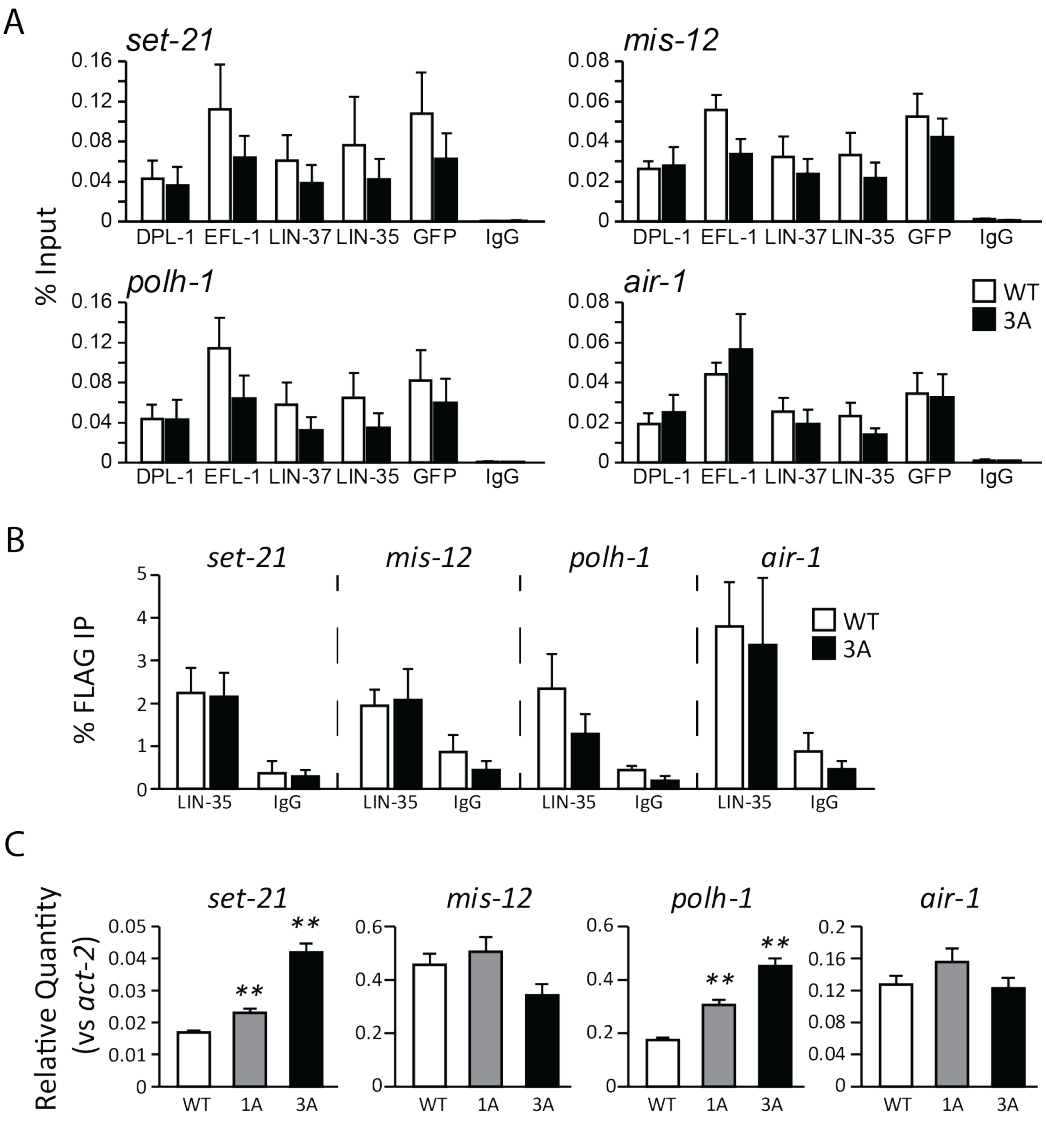

Table 1: Key Resources

REAGENT or RESOURCE	SOURCE	IDENTIFIER
Antibodies		
Rabbit polyclonal anti-LIN-35	SDIX/Novus	SDQ3232 / SDQ3233
Rabbit polyclonal anti-GFP	Novus Biologicals	NB600-308
Mouse monoclonal anti-FLAG, clone M2	Sigma Aldrich	F3165
Rabbit polyclonal DPL-1	SDIX/Novus	SDQ3599
Rabbit polyclonal EFL-1	SDIX/Novus	SDQ3490
Rabbit polyclonal LIN-37	SDIX/Novus	SDQ3166
Mouse Monoclonal anti-alpha-Tubulin, DM1A	Sigma Aldrich	T9026
Rabbit pre-immune serum (IgG)	-	-
Critical Commercial Assays		
NEBuilder HiFi DNA Assembly Master Mix	New England Biolabs	E2621
Q5 Site Directed Mutagenesis Kit	New England Biolabs	E0552
High-Capacity cDNA Reverse Transcription Kit	Applied Biosystems	4368813
Experimental Models: Organisms/Strains		
C. elegans Strain N2 (Bristol)	Caenorhabditis Genetics Center	N2
lin-52(bn132(lin-52p::TagRFP-T^SEC^3xflag::lin-52 3' UTR)) III / hT2G [bli-4(e937) let-?(q782) qIs48] (I:III)	This paper	SS1240
lin-52(bn133(lin-52p::TagRFP-T::3xflag::lin-52 3' UTR)) III / / hT2G [bli-4(e937) let-?(q782) qIs48] (I:III)	This paper	SS1241
lin-52(bn138(lin-52::GFP^SEC^3xflag)) III clone #1	This paper	SS1325
lin-52(bn138(lin-52::GFP^SEC^3xflag)) III clone #2	This paper	SS1326
lin-52(bn139(lin-52::GFP::3xflag)) III clone #1	This paper	SS1256
lin-52(bn139(lin-52::GFP::3xflag)) III clone #2	This paper	SS1257
lin-52(bn150(lin-52[C44A]::GFP::3xflag)) III clone #1	This paper	SS1273
lin-52(bn150(lin-52[C44A]::GFP::3xflag)) III clone #2	This paper	SS1274
lin-52(bn150(lin-52[C44A]::GFP::3xflag)) III clone #3	This paper	SS1275
lin-52(bn151(lin-52 [L42A,C44A,E46A]::GFP ::3xflag)) III clone #1	This paper	SS1276
lin-52(bn151(lin-52 [L42A,C44A,E46A]::GFP ::3xflag)) III clone #2	This paper	SS1277
lin-8(n2731)	Caenorhabditis Genetics Center, Harrison et al., 2007	MT10591 WormBase: WBVar00090564
lin-15A(n767)	Caenorhabditis Genetics Center, Huang et al., 1994	MT1806 WormBase: WBVar00089738
Oligonucleotides		
Primers for Cloning, RT-qPCR, and ChIP-qPCR, see Table S1	This paper	N/A
lin-52 mutagenesis 1A ssDNA template: CTTCGAATTTTAAATATTTTCAGAACAACAGAAAAAG ATGCTCGAggctACaGAAACAATGCCAGAAGAAAGTG AGCCAGTTCCAATGAAATGTC	This paper	N/A
lin-52 mutagenesis 3A ssDNA template: CTTCGAATTTTAAATATTTTCAGAACAACAGAAAAAG ATGgccGAAgctACagctACAATGCCAGAAGAAAGTGAG CCAGTTCCAATGAAATGTC	This paper	N/A

dpy-10(cn64) ssDNA template: CACTTGAACTTCAATACGGCAAGATGAGAATGACTGGAAACCGTACCGCATGCGGTGCCTATGGTAGCGGAGCTTCACATGGCTTCAGACCAACAGCCTA	Arribere et al, 2014	N/A
Recombinant DNA		
PU6::unc119_sgRNA vector	Friedland et al., 2013	Addgene Plasmid #46169
pDD284	Dickinson et al., 2015	Addgene Plasmid #66825
pDD162	Dickinson et al., 2013	Addgene Plasmid #47549
pCJF90 Pmyo-2::mCherry::unc-54utr	Frokjaer-Jensen et al, 2008	Addgene Plasmid #19327
pCFJ104 Pmyo-3::mCherry::unc-54utr	Frokjaer-Jensen et al, 2008	Addgene Plasmid #19328
pGH8 pRAB-3::mCherry::unc-54utr	Frokjaer-Jensen et al, 2008	Addgene Plasmid #19359
pPDG14 lin-52 5' sgRNA	This paper	N/A
pPDG18 lin-52 3' sgRNA	This paper	N/A
pPDG13 lin-52p::TagRFP-T^SEC^3xflag::lin-52 3' UTR	This paper	N/A
pPDG21 TagRFP-T 5' sgRNA-Cas9	This paper	N/A
pPDG22 TagRFP-T 3' sgRNA-Cas9	This paper	N/A
pPDG17 lin-52p::lin-52 CDS-GFP^SEC^3xflag::lin-52 3' UTR	This paper	N/A
pPDG59 lin-52 LxCxE sgRNA-Cas9	This paper	N/A
pJA58 dpy-10(cn64) sgRNA	Arribere et al., 2014	Addgene Plasmid #59933
Software and Algorithms		
ImageJ	Schneider et al., 2012	https://imagej.nih.gov/ij/
µManager	Edelstein et al., 2014	https://micro-manager.org/

Figure S1

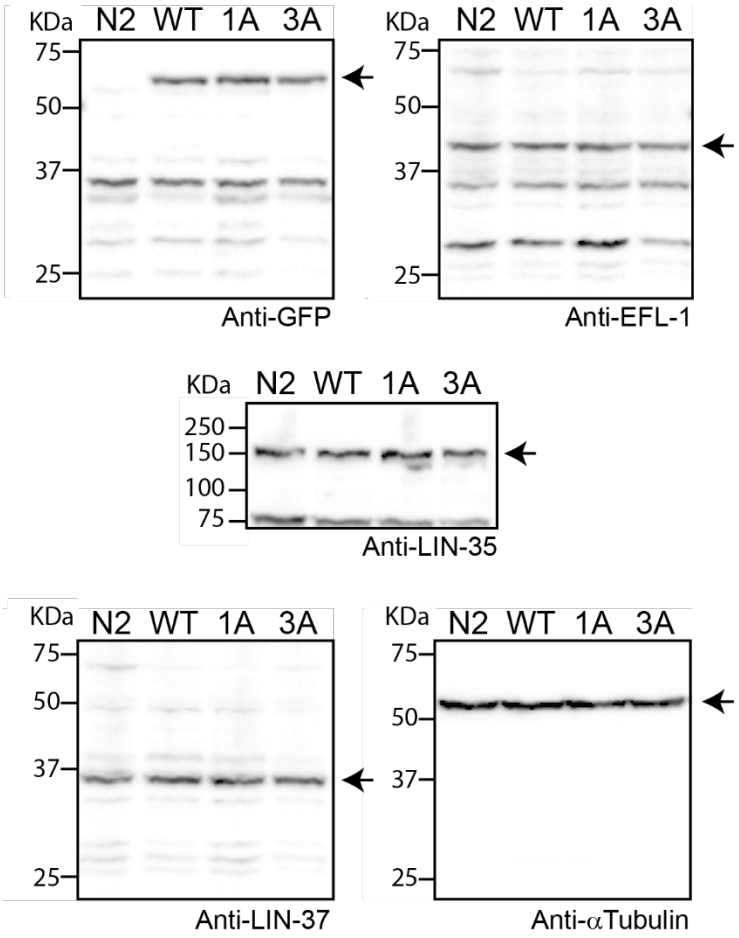

Figure S2

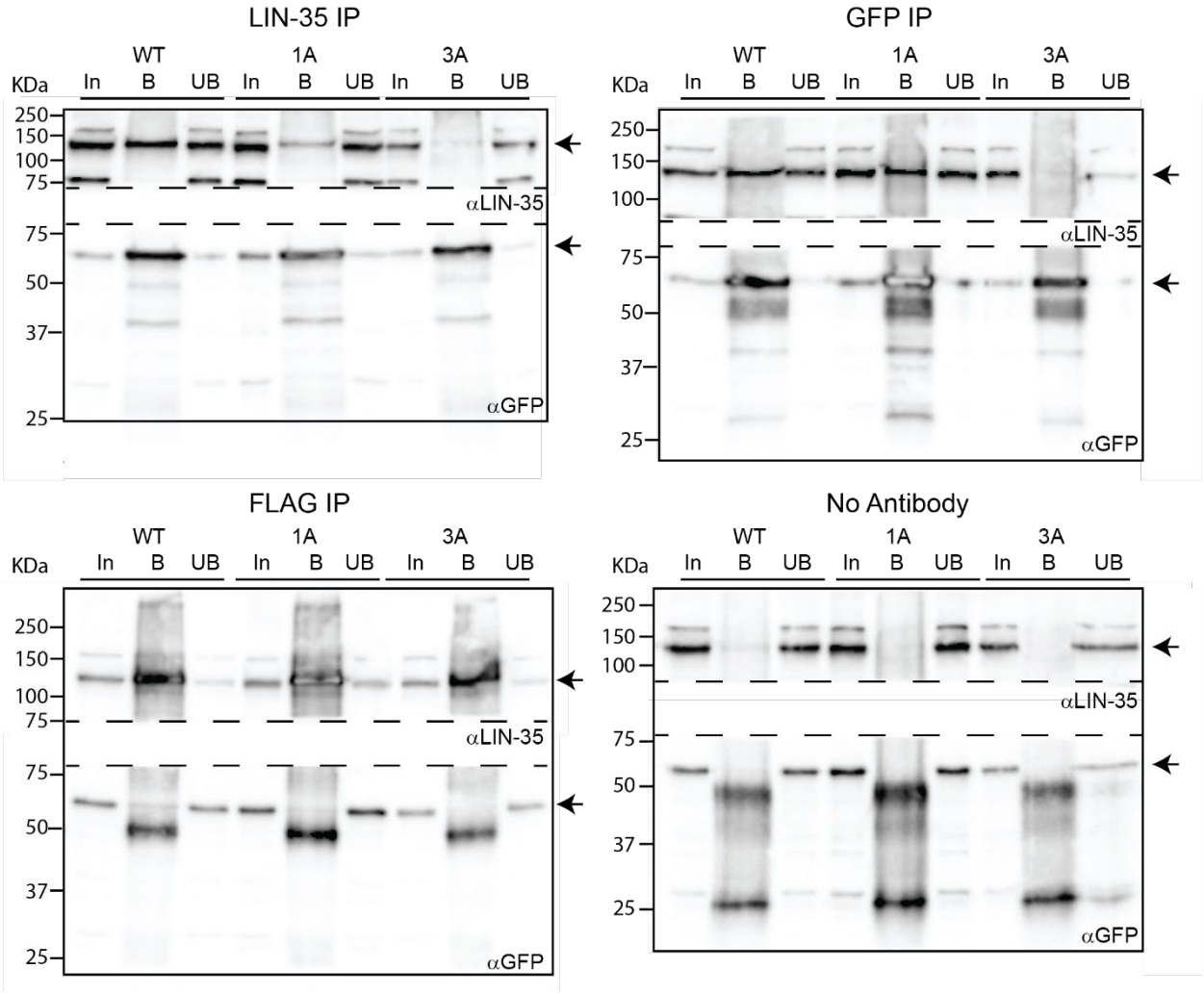

Figure S3

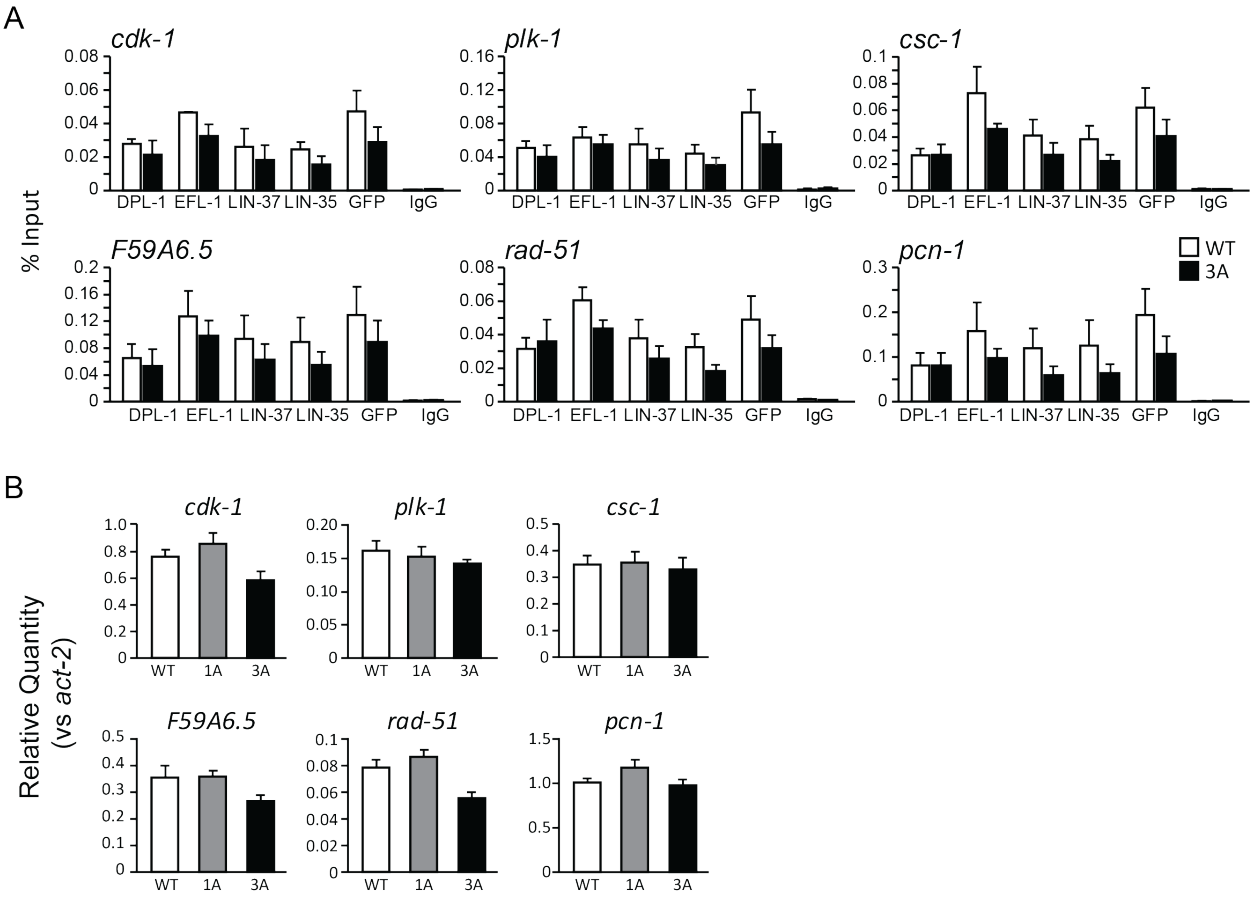

Table S1

Name	Sequence	Notes
Cloning Primers		
lin-52 gRNA 5' F	GTCGTATCCAATAAATCCTAGGTTTTAGAG CTAGAAATAGCAAGTTA	For pPDG14
lin-52 gRNA 5' R	CTAGGATTTATTGGATACGACAAACATTTAG ATTTGCAATTCAATTATATAG	For pPDG14
lin-52 gRNA 3' F	GAAGCCAGTGAATTGAATAGGTTTTAGAGC TAGAAATAGCAAGTTA	For pPDG18
lin-52 gRNA 3' R	CTATTCAATTCACTGGCTTCAAACATTTAGA TTTGCAATTCAATTATATAG	For pPDG18
lin-52_primer1_RFP	GTCACGACGTTGTAAAACGACGGCCAGTC GCATTCGAGCAAACCGGAGGA	For pPDG13
lin-52_primer2_RFP_Nterm	CTTGATGAGCTCCTCTCCCTTGGAGACCAT TTTTTTCCTGAAATTACCGCTATATGTC	For pPDG13
lin-52_primer3	CGTGATTACAAGGATGACGATGACAAGAGA ATTGAATAGTGGTCTATCAAAAAATAATG	For pPDG13 and pPDG17
lin-52_primer4_N-term	TCACACAGGAAACAGCTATGACCATGTTAT CACCTTGGGTACTTGCTGGAT	For pPDG13
lin-52_primer1_GFP	ACGTTGTAAAACGACGGCCAGTCGCCGGC ACATTCGAGCAAACCGGAGGA	For pPDG17
lin-52_primer2_C-term	CATCGATGCTCCTGAGGCTCCCGATGCTCC CTGGCTTCCTGTCGTTTCTTC	For pPDG17
lin-52_primer4_C-term	GGAAACAGCTATGACCATGTTATCGATTTC CACCTTGGGTACTTGCTGGAT	For pPDG17
sgRNA SDM R	CAAGACATCTCGCAATAGG	Reverse primer for Q5 targeted mutagenesis, see Dickinson et al, 2013
tagRFP-sgRNA SDM 5' F	TGGCTTTCCCTCTCCCTCGGGTTTTAGAGC TAGAAATAGCAAGT	For pPDG21
tagRFP-sgRNA SDM 3' F	TGTGTCCGAGCTTGGATGGGGTTTTAGAGC TAGAAATAGCAAGT	For pPDG22
lin-52 LxCxE sgRNA SDM F	ACTTTCTTCTGGCATTGTTTGTTTTAGAGCT AGAAATAGCAAGT	For pPDG59
ChIP-qPCR Primers		
set-21 Pro F	ACGACGGGCCCAAAAGTAAA	
set-21 Pro R	TGTTGTTTCGTTTTCGCGAATTT	
mis-12 Pro F	TTCCCGACAATTCGCTCTCC	
mis-12 Pro R	CGTGTATGCACACCTCACCT	
polh-1 Pro F	TCAATGTTTGAAACCCCGCC	
polh-1 Pro R	ATACTCAGCCAAGCAGCCAA	
air-1 Pro F	ATTCGCAACGTGTCAGCAAC	
air-1 Pro R	ATGAATTTTGCTTGGCGGGT	
cdk-1 Pro F	ACAATCCTTCTCAGCGCGT	
cdk-1 Pro R	CGATAGAAAAGGCGTAAGCGTG	
plk-1 Pro F	CGCTGTTTTGTTTAGCACCCT	
plk-1 Pro R	CAAGAGGCGAGCTGGAAACT	
csc-1 Pro F	TTTCCTTCTTTTGCGCGTGG	
csc-1 Pro R	CGGAGAAAATCGAATTTTTGAGGG	
F59A6.5 Pro F	GAAAACGGGTTCCGTATGCT	
F59A6.5 Pro R	TCTCTCTTCCGCAAACACCG	

rad-51 Pro F	GCGCACTTGCTGTACTCTTG	
rad-51 Pro R	CCGTTCCTATCGGTGCCTTT	
pcn-1 Pro F	TGAACGGAGAAAGTGCGATGA	
pcn-1 Pro F	GTTGCGCGTCAAATAAAATGCC	
RT-qPCR primers		
set-21 1359-1524 F	AAATGTTGCGCGAACTGTCG	
set-21 1359-1524 R	GTCCGTGTACGTCTTTCCGT	
mis-12 370-515 F	ATTCGACAGCTCCGCATCAA	
mis-12 370-515 R	ATTCGTGTTGGGCTATCGGG	
polh-1 759-842 F	TGTTCGAGGATTTGGCGGAA	
polh-1 759-842 R	TCCACTTCGAGCAGTTCACC	
air-1 594-740 F	ACGCCATACATTGTGCGGTA	
air-1 594-740 R	CCAGTTTGATTGGCGAACGG	
cdk-1 703-911 F	TTCAGAGTTCTCGGCACACC	
cdk-1 703-911 R	TTCGCGTTGAGACGAAGTGA	
plk-1 1050-1280 F	GAACAATGCCGATCGTGAGC	
plk-1 1050-1280 R	CCGATGCCATACTTGTCCGA	
csc-1 425-588 F	TTCCGATTGCTCCATCTGGC	
csc-1 425-588 R	CGAGAAGGCGATTTCCTCGT	
F59A6.5 (1964-2136) F	GCCAGATTGATGCGAAGCAG	
F59A6.5 (1964-2136) R	TTGACGTCTTTTCTCCGCGA	
rad-51 (534-686) F	CAATGCCACTTTTCGACCCG	
rad-51 (534-686) R	TCGGACATCATTGCTCCTGC	
pcn-1 (151-386) F	AAGTTGGAGGTCGGCCTTTT	
pcn-1 (151-386) R	ATCCCGAGATGTTCGCTGTC	

References

1. Classon, M., and Dyson, N. (2001). p107 and p130: versatile proteins with interesting pockets. Exp Cell Res *264*, 135-147.
2. Classon, M., and Harlow, E. (2002). The retinoblastoma tumour suppressor in development and cancer. Nat Rev Cancer *2*, 910-917.
3. Cobrinik, D. (2005). Pocket proteins and cell cycle control. Oncogene *24*, 2796-2809.
4. Dick, F.A., and Rubin, S.M. (2013). Molecular mechanisms underlying RB protein function. Nat Rev Mol Cell Biol *14*, 297-306.
5. Burkhart, D.L., and Sage, J. (2008). Cellular mechanisms of tumour suppression by the retinoblastoma gene. Nat Rev Cancer *8*, 671-682.
6. Cao, L., Peng, B., Yao, L., Zhang, X., Sun, K., Yang, X., and Yu, L. (2010). The ancient function of RB-E2F pathway: insights from its evolutionary history. Biol Direct *5*, 55.
7. Liban, T.J., Medina, E.M., Tripathi, S., Sengupta, S., Henry, R.W., Buchler, N.E., and Rubin, S.M. (2017). Conservation and divergence of C-terminal domain structure in the retinoblastoma protein family. Proc Natl Acad Sci U S A *114*, 4942-4947.
8. Litovchick, L., Sadasivam, S., Florens, L., Zhu, X., Swanson, S.K., Velmurugan, S., Chen, R., Washburn, M.P., Liu, X.S., and DeCaprio, J.A. (2007). Evolutionarily conserved multisubunit RBL2/p130 and E2F4 protein complex represses human cell cycle-dependent genes in quiescence. Mol Cell *26*, 539-551.
9. Hurford, R.K., Jr., Cobrinik, D., Lee, M.H., and Dyson, N. (1997). pRB and p107/p130 are required for the regulated expression of different sets of E2F responsive genes. Genes Dev *11*, 1447-1463.
10. Muller, G.A., Stangner, K., Schmitt, T., Wintsche, A., and Engeland, K. (2017). Timing of transcription during the cell cycle: Protein complexes binding to E2F, E2F/CLE, CDE/CHR, or CHR promoter elements define early and late cell cycle gene expression. Oncotarget *8*, 97736-97748.
11. Helin, K., Lees, J.A., Vidal, M., Dyson, N., Harlow, E., and Fattaey, A. (1992). A cDNA encoding a pRB-binding protein with properties of the transcription factor E2F. Cell *70*, 337-350.
12. Lees, J.A., Saito, M., Vidal, M., Valentine, M., Look, T., Harlow, E., Dyson, N., and Helin, K. (1993). The retinoblastoma protein binds to a family of E2F transcription factors. Mol Cell Biol *13*, 7813-7825.
13. Liban, T.J., Thwaites, M.J., Dick, F.A., and Rubin, S.M. (2016). Structural Conservation and E2F Binding Specificity within the Retinoblastoma Pocket Protein Family. J Mol Biol *428*, 3960-3971.
14. Korenjak, M., Taylor-Harding, B., Binne, U.K., Satterlee, J.S., Stevaux, O., Aasland, R., White-Cooper, H., Dyson, N., and Brehm, A. (2004). Native E2F/RBF complexes contain Myb-interacting proteins and repress transcription of developmentally controlled E2F target genes. Cell *119*, 181-193.
15. Lewis, P.W., Beall, E.L., Fleischer, T.C., Georlette, D., Link, A.J., and Botchan, M.R. (2004). Identification of a Drosophila Myb-E2F2/RBF transcriptional repressor complex. Genes Dev *18*, 2929-2940.
16. Harrison, M.M., Ceol, C.J., Lu, X., and Horvitz, H.R. (2006). Some C. elegans class B synthetic multivulva proteins encode a conserved LIN-35 Rb-containing complex distinct from a NuRD-like complex. Proc Natl Acad Sci U S A *103*, 16782-16787.
17. Goetsch, P.D., Garrigues, J.M., and Strome, S. (2017). Loss of the Caenorhabditis elegans pocket protein LIN-35 reveals MuvB's innate function as the repressor of DREAM target genes. PLoS Genet *13*, e1007088.
18. Guiley, K.Z., Liban, T.J., Felthousen, J.G., Ramanan, P., Litovchick, L., and Rubin, S.M. (2015). Structural mechanisms of DREAM complex assembly and regulation. Genes Dev *29*, 961-974.

19. Pilkinton, M., Sandoval, R., and Colamonici, O.R. (2007). Mammalian Mip/LIN-9 interacts with either the p107, p130/E2F4 repressor complex or B-Myb in a cell cycle-phase-dependent context distinct from the Drosophila dREAM complex. Oncogene *26*, 7535-7543.
20. Schmit, F., Korenjak, M., Mannefeld, M., Schmitt, K., Franke, C., von Eyss, B., Gagrica, S., Hanel, F., Brehm, A., and Gaubatz, S. (2007). LINC, a human complex that is related to pRB-containing complexes in invertebrates regulates the expression of G2/M genes. Cell Cycle *6*, 1903-1913.
21. Zwicker, J., Lucibello, F.C., Wolfraim, L.A., Gross, C., Truss, M., Engeland, K., and Muller, R. (1995). Cell cycle regulation of the cyclin A, cdc25C and cdc2 genes is based on a common mechanism of transcriptional repression. EMBO J *14*, 4514-4522.
22. Schmit, F., Cremer, S., and Gaubatz, S. (2009). LIN54 is an essential core subunit of the DREAM/LINC complex that binds to the cdc2 promoter in a sequence-specific manner. FEBS J *276*, 5703-5716.
23. Muller, G.A., and Engeland, K. (2010). The central role of CDE/CHR promoter elements in the regulation of cell cycle-dependent gene transcription. FEBS J *277*, 877-893.
24. Muller, G.A., Quaas, M., Schumann, M., Krause, E., Padi, M., Fischer, M., Litovchick, L., DeCaprio, J.A., and Engeland, K. (2012). The CHR promoter element controls cell cycle-dependent gene transcription and binds the DREAM and MMB complexes. Nucleic Acids Res *40*, 1561-1578.
25. Marceau, A.H., Felthousen, J.G., Goetsch, P.D., Iness, A.N., Lee, H.W., Tripathi, S.M., Strome, S., Litovchick, L., and Rubin, S.M. (2016). Structural basis for LIN54 recognition of CHR elements in cell cycle-regulated promoters. Nat Commun *7*, 12301.
26. Lu, X., and Horvitz, H.R. (1998). lin-35 and lin-53, two genes that antagonize a C. elegans Ras pathway, encode proteins similar to Rb and its binding protein RbAp48. Cell *95*, 981-991.
27. Boxem, M., and van den Heuvel, S. (2002). C. elegans class B synthetic multivulva genes act in G(1) regulation. Curr Biol *12*, 906-911.
28. Myers, T.R., and Greenwald, I. (2005). lin-35 Rb acts in the major hypodermis to oppose ras-mediated vulval induction in C. elegans. Dev Cell *8*, 117-123.
29. Cui, M., Chen, J., Myers, T.R., Hwang, B.J., Sternberg, P.W., Greenwald, I., and Han, M. (2006). SynMuv genes redundantly inhibit lin-3/EGF expression to prevent inappropriate vulval induction in C. elegans. Dev Cell *10*, 667-672.
30. Wang, D., Kennedy, S., Conte, D., Jr., Kim, J.K., Gabel, H.W., Kamath, R.S., Mello, C.C., and Ruvkun, G. (2005). Somatic misexpression of germline P granules and enhanced RNA interference in retinoblastoma pathway mutants. Nature *436*, 593-597.
31. Petrella, L.N., Wang, W., Spike, C.A., Rechtsteiner, A., Reinke, V., and Strome, S. (2011). synMuv B proteins antagonize germline fate in the intestine and ensure C. elegans survival. Development *138*, 1069-1079.
32. Dickinson, D.J., Pani, A.M., Heppert, J.K., Higgins, C.D., and Goldstein, B. (2015). Streamlined Genome Engineering with a Self-Excising Drug Selection Cassette. Genetics *200*, 1035-1049.
33. Ceol, C.J., Stegmeier, F., Harrison, M.M., and Horvitz, H.R. (2006). Identification and classification of genes that act antagonistically to let-60 Ras signaling in Caenorhabditis elegans vulval development. Genetics *173*, 709-726.
34. Mages, C.F., Wintsche, A., Bernhart, S.H., and Muller, G.A. (2017). The DREAM complex through its subunit Lin37 cooperates with Rb to initiate quiescence. Elife *6*.
35. Litovchick, L., Florens, L.A., Swanson, S.K., Washburn, M.P., and DeCaprio, J.A. (2011). DYRK1A protein kinase promotes quiescence and senescence through DREAM complex assembly. Genes Dev *25*, 801-813.
36. Arribere, J.A., Bell, R.T., Fu, B.X., Artiles, K.L., Hartman, P.S., and Fire, A.Z. (2014). Efficient marker-free recovery of custom genetic modifications with CRISPR/Cas9 in Caenorhabditis elegans. Genetics *198*, 837-846.

37. Chi, W., and Reinke, V. (2006). Promotion of oogenesis and embryogenesis in the C. elegans gonad by EFL-1/DPL-1 (E2F) does not require LIN-35 (pRB). Development *133*, 3147-3157.
38. Tabuchi, T.M., Deplancke, B., Osato, N., Zhu, L.J., Barrasa, M.I., Harrison, M.M., Horvitz, H.R., Walhout, A.J., and Hagstrom, K.A. (2011). Chromosome-biased binding and gene regulation by the Caenorhabditis elegans DRM complex. PLoS Genet *7*, e1002074.
39. Beitel, G.J., Lambie, E.J., and Horvitz, H.R. (2000). The C. elegans gene lin-9,which acts in an Rb-related pathway, is required for gonadal sheath cell development and encodes a novel protein. Gene *254*, 253-263.
40. Ceol, C.J., and Horvitz, H.R. (2001). dpl-1 DP and efl-1 E2F act with lin-35 Rb to antagonize Ras signaling in C. elegans vulval development. Mol Cell *7*, 461-473.
41. Fay, D.S., and Yochem, J. (2007). The SynMuv genes of Caenorhabditis elegans in vulval development and beyond. Dev Biol *306*, 1-9.
42. Harrison, M.M., Lu, X., and Horvitz, H.R. (2007). LIN-61, one of two Caenorhabditis elegans malignant-brain-tumor-repeat-containing proteins, acts with the DRM and NuRD-like protein complexes in vulval development but not in certain other biological processes. Genetics *176*, 255-271.
43. Huang, L.S., Tzou, P., and Sternberg, P.W. (1994). The lin-15 locus encodes two negative regulators of Caenorhabditis elegans vulval development. Mol Biol Cell *5*, 395-411.
44. Tao, Y., Kassatly, R.F., Cress, W.D., and Horowitz, J.M. (1997). Subunit composition determines E2F DNA-binding site specificity. Mol Cell Biol *17*, 6994-7007.
45. Kirienko, N.V., and Fay, D.S. (2007). Transcriptome profiling of the C. elegans Rb ortholog reveals diverse developmental roles. Dev Biol *305*, 674-684.
46. Dyson, N.J. (2016). RB1: a prototype tumor suppressor and an enigma. Genes Dev *30*, 1492-1502.
47. Rubin, S.M. (2013). Deciphering the retinoblastoma protein phosphorylation code. Trends Biochem Sci *38*, 12-19.
48. Narasimha, A.M., Kaulich, M., Shapiro, G.S., Choi, Y.J., Sicinski, P., and Dowdy, S.F. (2014). Cyclin D activates the Rb tumor suppressor by mono-phosphorylation. Elife *3*.
49. Friedland, A.E., Tzur, Y.B., Esvelt, K.M., Colaiacovo, M.P., Church, G.M., and Calarco, J.A. (2013). Heritable genome editing in C. elegans via a CRISPR-Cas9 system. Nat Methods *10*, 741-743.
50. Gibson, D.G., Young, L., Chuang, R.Y., Venter, J.C., Hutchison, C.A., 3rd, and Smith, H.O. (2009). Enzymatic assembly of DNA molecules up to several hundred kilobases. Nat Methods *6*, 343-345.
51. Frokjaer-Jensen, C., Davis, M.W., Hopkins, C.E., Newman, B.J., Thummel, J.M., Olesen, S.P., Grunnet, M., and Jorgensen, E.M. (2008). Single-copy insertion of transgenes in Caenorhabditis elegans. Nat Genet *40*, 1375-1383.
52. McKim, K.S., Peters, K., and Rose, A.M. (1993). Two types of sites required for meiotic chromosome pairing in Caenorhabditis elegans. Genetics *134*, 749-768.
53. Dickinson, D.J., Ward, J.D., Reiner, D.J., and Goldstein, B. (2013). Engineering the Caenorhabditis elegans genome using Cas9-triggered homologous recombination. Nat Methods *10*, 1028-1034.
54. Kim, E., Sun, L., Gabel, C.V., and Fang-Yen, C. (2013). Long-term imaging of Caenorhabditis elegans using nanoparticle-mediated immobilization. PLoS One *8*, e53419.
55. Edelstein, A.D., Tsuchida, M.A., Amodaj, N., Pinkard, H., Vale, R.D., and Stuurman, N. (2014). Advanced methods of microscope control using muManager software. J Biol Methods *1*.
56. Schneider, C.A., Rasband, W.S., and Eliceiri, K.W. (2012). NIH Image to ImageJ: 25 years of image analysis. Nat Methods *9*, 671-675.